A Study into the ADP-Ribosylome of IFN-γ-Stimulated THP-1 Human Macrophage-like Cells Identifies ARTD8/PARP14 and ARTD9/PARP9 ADP-Ribosylation

Hideyuki Higashi,[†] Takashi Maejima,[†] Lang Ho Lee,[†] Yukiyoshi Yamazaki,[†] Michael O. Hottiger,[‡] Sasha A. Singh,*[,†,#] and Masanori Aikawa*[,†,§,||,#]

[†]Center for Interdisciplinary Cardiovascular Sciences, Division of Cardiovascular Medicine, Department of Medicine, Brigham Women's Hospital, Harvard Medical School, Boston, Massachusetts 02115, United States

[‡]Department of Molecular Mechanisms of Disease, University of Zurich, 8057 Zurich, Switzerland

[§]Center for Excellence in Vascular Biology, Cardiovascular Division, Brigham Women's Hospital, Harvard Medical School, Boston, Massachusetts 02115, United States

[||]Channing Division of Network Medicine, Department of Medicine, Brigham Women's Hospital, Harvard Medical School, Boston, Massachusetts 02115, United States

Ⓢ *Supporting Information*

ABSTRACT: ADP-ribosylation is a post-translational modification that, until recently, has remained elusive to study at the cellular level. Previously dependent on radioactive tracers to identify ADP-ribosylation targets, several advances in mass spectrometric workflows now permit global identification of ADP-ribosylated substrates. In this study, we capitalized on two ADP-ribosylation enrichment strategies, and multiple activation methods performed on the Orbitrap Fusion Lumos, to identify IFN-γ-induced ADP-ribosylation substrates in macrophages. The ADP-ribosyl binding protein, Af1521, was used to enrich ADP-ribosylated peptides, and the antipoly-ADP-ribosyl antibody, 10H, was used to enrich ADP-ribosylated proteins. ADP-ribosyl-specific mass spectra were further enriched by an ADP-ribose product ion triggered EThcD and HCD activation strategy, in combination with multiple acquisitions that segmented the survey scan into smaller ranges. HCD and EThcD resulted in overlapping and unique ADP-ribosyl peptide identifications, with HCD providing more peptide identifications but EThcD providing more reliable ADP-ribosyl acceptor sites. Our acquisition strategies also resulted in the first ever characterization of ADP-ribosyl on three poly-ADP-ribose polymerases, ARTD9/PARP9, ARTD10/PARP10, and ARTD8/PARP14. IFN-γ increased the ADP-ribosylation status of ARTD9/PARP9, ARTD8/PARP14, and proteins involved in RNA processes. This study therefore summarizes specific molecular pathways at the intersection of IFN-γ and ADP-ribosylation signaling pathways.

KEYWORDS: higher-energy collision dissociation (HCD), electron transfer higher-energy collision dissociation (EThcD), Orbitrap Fusion Lumos, gas phase segmentation, parallel reaction monitoring (PRM), proteomics, post-translational modification (PTM)
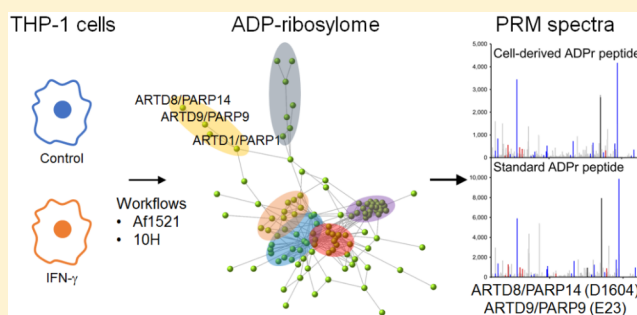
■ INTRODUCTION

ADP-ribosylation is a post-translational modification (PTM) known to regulate several biological processes including DNA repair, transcription, translation, and cell signaling.[1] The modification is reversibly regulated by the attachment and degradation of ADP-ribose units on protein substrates. ADP-ribosylation, either by formation of mono- or poly-ADP-ribose units, is catalyzed by the diphtheria toxin-like ADP-ribosyltransferases (ARTDs) that are also known as the poly-ADP-ribose polymerases (PARPs). Seventeen members comprise the ARTD/PARP family;[2] however, only ARTD1/PARP1, ARTD2/PARP2, ARTD5/PARP5A, and ARTD6/

PARP5B catalyze poly-ADP-ribosylation reactions (PARylation), whereas the remaining catalyze mono-ADP-ribosylation reactions (MARylation) or are inactive.[3] The ARTD/PARP enzymes transfer the ADP-ribosyl (ADPr) moiety of NAD$^+$ to protein substrates forming either a carboxylate ester bond with aspartate or glutamate (D, E), a nitrogen-glycosidic bond with arginine or lysine (R, K), or, as demonstrated very recently, an oxygen-glycosidic bond with serine (S).[4,5] On the other hand, ADP-ribosylation removal is catalyzed by poly(ADP-ribose)

glycohydrolase (PARG),[6] ADP-ribosylhydrolase 3 (ARH3),[7] macrodomains-containing proteins such as MacroD1 and MacroD2,[8] and terminal ADP-ribose protein glycohydrolase TARG1/C6orf130.[9]

Previous to mass spectrometry-based methods, most studies that identified ADP-ribosylation substrates were performed in a targeted manner, for instance, using radioactive tracers such as [³H]NAD⁺. Histones and other nuclear proteins such as elongation factor 2 were the first bacterial ADP-ribosylation substrates to be identified.[10,11] Recently, through vigorous ADPr proteins/peptides purification and enrichment studies, global ADP-ribosylation proteomics is now feasible.[12−14] Specifically, ADPr enrichment can be done at the peptide level using a workflow that first simplifies PARylation to MARylation by treating peptides with PARG. This step is necessary since the acidic ADPr polymer cannot ionize in positive mode, whereas the monomeric form is detectable using standard mass spectrometry acquisition methods (more below).[15] The second step enriches MARylated peptides via binding to Af1521, an ADPr-binding protein from *Archaeoglobus fulgidus*.[12,16] Additional ADP-ribosylation proteomics strategies include purification of PARylated proteins using the 10H antibody that was raised against more than 20 ADP-ribose residues.[17] ADPr proteins are then inferred on the basis of their presence in the enriched proteome; however, this enrichment strategy cannot differentiate between ADPr protein substrates and their coenriched binding partners.[18−21]

For the detection of MARylated peptides, one or multiple acquisition methods can be used for their sequencing, most optimally using higher-energy collision dissociation (HCD), electron transfer dissociation (ETD), and/or electron transfer/higher-energy collision dissociation (EThcD).[22−25] In one such example performed on an Orbitrap Fusion platform, the most abundant four ADPr fragment ions (136.06, 250.09, 348.07, and 428.04 m/z) were used to execute product ion triggered data acquisitions that employed high energy, low resolution HCD scans for ADPr product ion screening, followed by lower energy, higher resolution EThcD and HCD scans for peptide backbone sequencing.[26] The availability of hybrid, high resolution and mass accuracy instruments therefore contribute to the feasibility of performing global ADP-ribosylation proteomics studies. Despite these recent advances, robust automated ADPr annotation methods are still lacking; thus, a considerable amount of manual validation is required.[27]

To date, most ADP-ribosylation proteomics studies have been geared toward identifying oxidative stress-induced PARylation substrates. Proteins involved in, for instance, transcription regulation, DNA repair, DNA replication, and chromosome organization have been identified to be ADP-ribosylated.[28,29] Due to the significant impact of ARTDs/PARPs on DNA repair, transcription, and cell cycling,[30] these enzymes have generated an active area of anticancer therapeutic research.[31] Outside of cancer-focused research, little is known about ADP-ribosylation biology in general; however, there is growing interest in the field of immunology. The first observed relationship between ADP-ribosylation and pro-inflammatory signaling in macrophages dates back to the 1980s.[32−34] For instance, radioactive tracer studies and immunostaining using a preform of the 10H antibody[35] in human monocyte-derived macrophages demonstrated that IFN-γ increased accumulation of PARylated protein signal in nuclei.[32] Moreover, the mRNA of ARTD1/PARP1, the major

ADP-ribosylating enzyme studied at that time, did not change in response to IFN-γ, suggesting other mechanisms, independent of ARTD1/PARP1 levels, for the increase in total ADP-ribosylation.[32]

Since these landmark studies, others have investigated ADP-ribosylation in immune cell biology, proposing that cytokine and oxidative stressors activate ARTD1/PARP1, driving a PARylation signature.[36,37] However, the mRNA and protein levels of the lesser abundant mono-ADP-ribosylating enzymes ARTD10/PARP10, ARTD12/PARP12, ARTD8/PARP14, and the enzymatically inactive ARTD9/PARP9, are induced in response to various cytokines including IFN-γ.[38−40] Specifically, using a global proteomics analysis we determined that IFN-γ induces ARTD8/PARP14 and ARTD9/PARP9 proteins in the human macrophage-like cell line, THP-1.[41] Nonetheless, differentiating the global consequences of their enzyme activities from the ubiquitous PARylation activity of ARTD1/PARP1 is challenging, since commonly applied ADP-ribosylation workflows favor the polymerized form of the modification.[35,37] Evidence independent of ADP-ribosylation activity, including in vitro and in vivo genetic deletion indicate the anti-inflammatory properties of ARTD8/PARP14. For instance, genetic deletion of ARTD8/PARP14 in three mouse models of arterial disease, including bone-marrow transplantation from deficient mice, accelerated arterial lesion development and pro-inflammatory activation of macrophages.[41] While the roles of these MARylation enzymes appear to be independent of DNA repair,[42] their precise roles in macrophage activation is not fully known. In addition, no studies have investigated a macrophage ADP-ribosylome. We therefore performed a global ADP-ribosylation study on the IFN-γ-treated THP-1 cells, using two independent approaches (Af1521 and 10H antibody) to characterize the baseline ADP-ribosylome and monitor its changes in response to this cytokine.

■ EXPERIMENTAL SECTION

Cell Culture Conditions

THP-1 cells, a human monocytic cell line derived from an acute monocytic leukemia patient, were purchased from American Type Culture Collection (ATCC, Manassas, VA, Cat# TIB-202) and maintained in Roswell Park Memorial Institute (RPMI) 1640 medium (VWR International, Radnor, PA, Cat# 12001-590) in 10% fetal bovine serum (Fisher Scientific, Pittsburgh, PA, Cat# 1600044) with penicillin and streptomycin (VWR International, Cat# 45000-652) at 37 °C in 5% CO_2. THP-1 cells were differentiated from their monocyte-like state into macrophages using RPMI supplemented with phorbol 12-myristate 13-acetate (PMA, 100 ng/mL, Sigma-Aldrich, St. Louis, MO, Cat# P8139) for 2 days, followed by a media exchange back to RPMI alone for subsequent activation experiments.

IFN-γ Stimulation of THP-1 Cells

THP-1 cells were treated with IFN-γ (10 ng/mL, R&D Systems, Minneapolis, MN, Cat# 285-IF) for the indicated times below. After treatment with IFN-γ, cells were washed with phosphate buffered saline (PBS, VWR International, Cat# 12001-680), and then the cells were harvested for subsequent experiments.

Auto-MARylation of ARTD8/PARP14, and ARTD8/PARP14-Catalyzed MARylation of STAT1 and ARTD9/PARP9

ARTD8/PARP14 recombinant human protein (amino acids 1470−1801, catalytic domain only; 4.0 μg, BPS Bioscience, San Diego, CA, Cat# 80514) alone, and 1.0 μg of ARTD8/PARP14 with signal transducer and activator of transcription 1 (STAT1) recombinant human protein (4.0 μg, Thermo Fisher Scientific, Waltham, MA, Cat# PHF0011) were incubated in a reaction buffer [50 μM β-nicotinamide adenine dinucleotide (β-NAD, Sigma-Aldrich, Cat# N0632), 50 mM Tris-HCl pH 7.4 (Boston Bio Products, Ashland, MA, Cat# BM-314)] for 1 h at room temperature. The ADP-ribosylation reaction was stopped by adding 2X-Laemmli buffer (Boston Bio Products, Cat# BP-111R), and the proteins were boiled at 95 °C for 5 min. The MARylated ARTD8/PARP14 and STAT1 proteins were used for liquid chromatography tandem mass spectrometry (LC−MS/MS) analysis (see in In-Gel Proteolysis and Peptide Sample Preparation). ARTD9/PARP9 recombinant human protein (4.0 μg, BPS Bioscience, Cat# 80509) was boiled at 95 °C for 5 min to inactivate the enzyme's inhibitory action against ARTD8/PARP14.[41] The protein was incubated with 4.0 μg of ARTD8/PARP14 in a high β-NAD reaction buffer (1 mM β-NAD and 50 mM Tris-HCl pH 7.4) for 1 h at room temperature. The ADP-ribosylation reaction was stopped by adding the Lyse Buffer included in the iST proteolysis kit (PreOmics GmbH, Planegg/Martinsried, Germany, Cat# P.O.00027), and the MARylated ARTD9/PARP9 protein was digested according to the iST protocol. The MARylated ARTD9/PARP9 peptides were used for LC−MS/MS.

Af1521-Dependent Enrichment of MARylated Peptides

Expression and purification of the Af1521 macrodomain were done according to a published protocol.[43] THP-1 cells were treated with or without IFN-γ (10 ng/mL) for 6 h (15 10 cm-dishes per treatment), and then lysed in modified RIPA buffer [50 mM Tris-HCl pH 7.4, 0.4 M NaCl (Sigma-Aldrich, Cat# S9888), 1.0 mM EDTA (Boston Bio Products, Cat# BM-150), 1.0% nonidet P-40 (Sigma-Aldrich, Cat# 74385), 0.1% sodium deoxycholate (Sigma-Aldrich, Cat# D6750), 40 μM PJ34 (Millipore Sigma, Cat# 528150), 1.0 μM ADP-HPD (Millipore Sigma, Cat# 118415), protease inhibitor cocktail (Sigma-Aldrich, Cat# P8340)] as written previously.[43] After cell lysis and acetone (Fisher Scientific, Cat# A949-1) precipitation, 15 mg of proteins were digested with LysC (FUJIFILM Wako Pure Chemical, Osaka, Japan, Cat# 125-05061) for 4 h, followed by trypsin (Promega, Madison, WI, Cat# V5280) in 20 mM ammonium bicarbonate (Sigma-Aldrich, Cat# 09830) overnight. The peptides were desalted using Sep-Pak C18 Classic Cartridge (Waters, Milford, MA, Cat# WAT051910) by following the manufacturer's instructions. Using a tabletop speed vacuum (Thermo Fisher Scientific, Cat# SPD1010), the peptide sample was reduced to a final volume of 0.8 mL of 1× affinity precipitation buffer [50 mM Tris-HCl pH 7.4, 10 mM MgCl$_2$ (Sigma-Aldrich, Cat# 63069), 250 μM dithiothreitol (DTT, Thermo Fisher Scientific, Cat# 20290), 50 mM NaCl]. Peptide amount was determined by using a NanoDrop2000 Spectrophotometer at 280 nm (Thermo Fisher Scientific). One hundred microgram input peptide was set aside, whereas 10 mg of peptide was used for the Af1521 enrichment protocol. The peptide mixture was treated with PARG (Creative BioMart, Shirley, NY, Cat# PARG-31H) to obtain only MARylated peptides, and the

peptides were enriched using the macrodomain affinity pull-down as described previously.[43] The peptides were desalted using Oasis HLB cartridge (Waters, Cat# 186008055) by following its instruction and suspended in loading buffer [5.0% acetonitrile (Fisher Scientific, Cat# A955-1), 0.5% formic acid (Thermo Fisher Scientific, Cat# 28905) in water (Fisher Scientific, Cat# W6-1)] for LC−MS/MS analysis.

Anti-PARylation Immunoprecipitation (10H Antibody) and Anti-ADPr Protein Enrichment (Af1521 Macrodomain)

Control and IFN-γ-activated THP-1 cells were prepared by incubating the cells with or without IFN-γ (10 ng/mL) for 6 h. In addition to the two conditions, THP-1 cells were pretreated with 20 μM PJ34 (pan-ARTD/PARP inhibitor; EMD Biosciences, Burlington, MA, Cat# 528150, 5 mg) for 12 h, and then treated with IFN-γ (10 ng/mL) for 6 h. The cells were lysed in cell lysis buffer [20 mM HEPES (pH 7.5) (Boston Bio Products, Cat# BB-107), 0.1 M KCl (Sigma-Aldrich, Cat# P9333-500G), 0.2 mM EDTA, 10% glycerol (VWR International, Cat# BDH1172-1LP), 0.1% nonidet P-40, protease inhibitor cocktail, phosphatase inhibitor (Sigma-Aldrich, Cat# 049068450), 40 μM PJ34]. The lysates were sonicated using a Branson analog sonifier 450 (Branson Ultrasonics, Danbury, CT, Cat# 101063198) with the following settings—5 pulse, cycle 50% for 1 min—and then centrifuged at 12 000 rpm for 15 min at 4 °C. The soluble fraction was used for immunoblotting. Protein concentration was measured using the bicinchoninic acid (BCA) method (Thermo Fisher Scientific, Cat# 23225).

Immunoprecipitation (IP, 10H Antibody). To obtain the minimum IP input of 1.0 mg protein, cell lysate was prepared from three 10 cm-dishes. We added 10 μg of 10H anti-ADP-ribose antibody (Millipore Sigma, Cat# MAB3192) that recognizes primarily PARylated proteins, or 10 μg of mouse IgG (Sigma-Aldrich, Cat# I5381-1MG). The lysates were then incubated for 30 min at 4 °C using a rotator, followed by the addition of 25 μL of Dynabeads Protein G (Thermo Fisher Scientific, Cat# 10004D), and incubated for another hour at 4 °C. The beads were washed with cell lysis buffer three times. To elute the bound proteins, we added 25 μL of 2X-Laemmli buffer and boiled the samples for 5 min at 95 °C. The eluate was used for immunoblot analysis (5 μL, see Immunoblotting) and LC−MS/MS analysis (20 μL, see In-Gel Proteolysis and Peptide Sample Preparation).

ADPr Protein Enrichment (Af1521 Macrodomain). Cell lysate from three 10 cm-dishes (1.0 mg) was incubated with 150 μL of Af1521 macrodomain conjugated to Glutathione sepharose 4B (GE Healthcare, Chicago, IL, Cat# 17075601)[43] for 90 min at 4 °C using a rotator. To elute the bound proteins, we added 25 μL of 2X-Laemmli buffer and boiled the samples for 5 min at 95 °C. The eluate was used for immunoblot analysis (see Immunoblotting).

Immunoblotting. The sample eluate from above was separated by SDS-PAGE [8.0% acrylamide (Boston Bio Products, Cat# BAC-30PA), BAC-30PA (Boston Bio Products, Cat# BP-90), stacking buffer (Boston Bio Products, Cat# BP-95), N,N,N′,N′-tetramethylethylenediamine (TEMED, Sigma-Aldrich, Cat# 1610801), ammonium persulfate (Sigma-Aldrich, Cat# A3678-25G)] and transferred to nitrocellulose membrane (Bio-Rad Laboratories, Hercules, CA, Cat# 1620112). The following primary antibodies were used: a human ARTD8/PARP14 antibody (1:1000, Santa Cruz Biotechnology, Cat# sc-377150); the antibody for human

ARTD9/PARP9 produced in rat was custom-made by Aldevron (1:250, Freiburg, Germany, CloneIDs 5G1 and 1B4); a pan ADP-ribose reagent (1:300, Millipore Sigma, Cat# MABE1016); a human ARTD1/PARP1 antibody (1:1000, Thermo Fisher Scientific, Cat# PA5-34803); a human α-tubulin antibody (1:1000, Sigma-Aldrich, Cat# B-5-1-2); a human 60 kDa heat shock protein, mitochondrial (HSPD1) antibody (1:1000, Thermo Fisher Scientific, Cat# MA3-012); a human glyceraldehyde-3-phosphate dehydrogenase (GAPDH) antibody (1:1000, Thermo Fisher Scientific, Cat# MA5-15738). The secondary antibodies were antimouse peroxidase conjugate (1:5000, Sigma-Aldrich, Cat# A4416-1ML), anti-rabbit peroxidase conjugate (1:5000, Sigma-Aldrich, Cat# A0545-1ML) or antirat peroxidase conjugate (1:5000, Sigma-Aldrich, Cat# A9037-1ML) as required for the primary and detected using Clarity Western ECL blotting substrate (Bio-Rad Laboratories, Cat# 1705060) and imaged using the ImageQuant LAS 4000 (GE Healthcare).

In-Gel Proteolysis and Peptide Sample Preparation

The MARylated ARTD8/PARP14, ARTD8/PARP14-MARylated STAT1, and the 10H IP eluates were separated by SDS-PAGE. The gels were washed in water for 5 min three times, incubated with Bio-Safe Coomassie G-250 Stain (Bio-Rad Laboratories, Cat# 1610786) for 1 h, and washed with water for 30 min. For the MARylated ARTD8/PARP14 and STAT1, the molecular weight window around ARTD8/PARP14 (67 kDa) and STAT1 (~90 kDa) were excised. For the 10H IP eluates, each SDS-PAGE lane was cut into 11 fractions and washed with 100 mM ammonium bicarbonate, then reduced in 5 mM DTT for 45 min at 55 °C, alkylated in 30 mM iodoacetamide (Sigma-Aldrich, Cat# I1149) for 45 min with protection from light, and digested with trypsin for 4 h at 37 °C. Peptides were extracted by adding acetonitrile. Samples were dried down using a tabletop speed vacuum and suspended in loading buffer (5.0% acetonitrile, 0.5% formic acid in water) for LC–MS/MS analysis.

LC–MS/MS Analysis

All peptide samples were analyzed on an Orbitrap Fusion Lumos mass spectrometer fronted with an EASY-Spray Source, coupled to an Easy-nLC1000 HPLC pump (Thermo Fisher Scientific). The peptides were subjected to a dual column setup: an Acclaim PepMap RSLC C18 trap column, 75 μm × 20 mm (Thermo Fisher Scientific, Cat# 164261); and an EASY-Spray LC Column, 75 μm × 250 mm (Thermo Fisher Scientific, Cat# ES802). The analytical gradient was run at 300 nL/min from 5 to 21% Solvent B (acetonitrile/0.1% formic acid) for 50 min, 21 to 30% Solvent B for 10 min, and 95% Solvent B for 5 min. Solvent A was water/0.1% formic acid.

Af1521-Dependent Enrichment of MARylated Peptides. Each peptide sample was analyzed five times: a full scan range of 400−1500 m/z and four gas phase segmentation (GPS) scans;[44] 400−605, 595−805, 795−1005, and 995−1200 m/z in order to increase signal-to-noise ratio. The instrument was set to 120 K resolution and the top N precursor ions in 3 s cycle time (30 s dynamic exclusion enabled) were subjected to MS/MS acquisitions. For MS/MS, an ADP-ribose product ion triggered method was applied.[26] The method includes data-dependent HCD acquisition (collision energy 35% ± 5.0%, isolation width 1.6 m/z, and resolution set to 30 K), followed by EThcD (calibrated charge dependent ETD parameters enabled, supplemental activation collision energy 25%, and resolution set to 120 K) and HCD

(collision energy 30% ± 5.0%, and resolution set to 120 K) data acquisitions when two or more ADPr fragment ions (136.0623, 250.0940, 348.0709, and 428.0372 m/z) were observed in the first HCD scan. Af1521 input peptides were analyzed using the same product ion triggered method as for enriched peptides, however, only using MS1 scan range of 400−1500 m/z. Of note, we did not identify any ADPr peptides in the input samples. The initial acquisition method was verified using the cell-free derived ADPr STAT1 peptide (VMAAENIPENPLK, E5-ADPr, precursor ion 983.9045 m/z, z = 2), was isolated (isolation width 1.6 m/z) and subjected to HCD with the five different collision energies (15, 25, 35, 45, 55% ±5.0%), and resolution was set to 120 K for MS/MS.

Parallel Reaction Monitoring (PRM). ADPr peptides identified in the ARTD8/PARP14 auto-ADP-ribosylation and trans-ADP-ribosylation of ARTD9/PARP9 reactions (data-dependent acquisition, DDA followed by PRM for high quality spectra) were used to validate their cognates identified from THP-1 experiments. ADPr peptides enriched from IFN-γ-stimulated THP-1 cells were reinjected for PRM (Figure S1). The targeted peptides were isolated (isolation width 0.8 m/z) and subjected to either EThcD (calibrated charge dependent ETD parameters enabled, supplemental activation collision energy 25%, and resolution set to 500 K) or HCD (collision energy 30% ± 5.0%, and resolution set to 500 K) for MS/MS.

10H-Dependent Anti-PARylated Immunoprecipitated Peptides. The instrument was set to 120 K resolution, and the top N precursor ions in 3 s cycle time (30 s dynamic exclusion enabled) were subjected to HCD (collision energy 30% ± 5.0%, isolation width 1.6 m/z, and resolution set to 30 K) for MS/MS. DDAs of ADPr peptide standards were also done by this data acquisition method (Figure S1).

LC–MS/MS Data Analysis

ARTD8/PARP14-MARylated STAT1 Peptide. To calculate the area under the curve (AUC) of four ADPr fragment ions (136.0623, 250.0940, 348.0709, and 428.0372 m/z)[22] from the MARylated STAT1 peptide (VMAAENIPENPLK, E5-ADPr, precursor ion 983.9045 m/z, z = 2), the MS/MS raw files were loaded to the Skyline software (https://skyline.gs.washington.edu). The fragment ions eluted at 48.5 ± 0.5 min and allowed mass tolerance within ±3.5 ppm were used for the calculation. The AUC of each fragment ion was exported from the software.

Af1521-Dependent Enrichment of MARylated Peptides. The MS/MS spectra that include ADPr fragment ions were extracted by a scan event filter, then EThcD and HCD spectra were separately queried against the human UniProt database (downloaded on August 1, 2014) using the SEQUEST-HT search algorithm, via the Proteome Discoverer (PD) Package (version 2.2, Thermo Fisher Scientific). The precursor peaks and ADPr fragment ions at 136.0623, 250.0940, 348.0709, and 428.0372 ± 0.005 m/z were excluded by a nonfragment filter. Trypsin was set to a digestion enzyme allowing up to four miss cleavages, using 10 ppm precursor tolerance window and 0.02 Da fragment tolerance window. ADPr (+541.061 Da) of D, E, K, R, and S, and oxidation (+15.995 Da) of methionine (M) were set as variable modifications, and carbamidomethylation (+57.021 Da) of cysteine (C) was set as a fixed modification. The peptide false discovery rate (FDR) was calculated using Percolator provided by PD and peptides were filtered based on a 1.0% FDR. The ptmRS was used to calculate PTM site probabilities. Only the
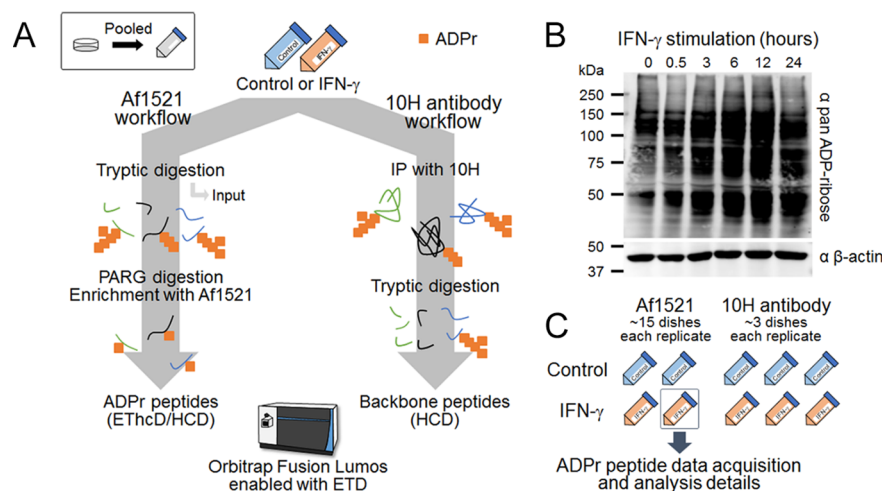
Figure 1. ADP-ribosylation increases during IFN-γ-induced pro-inflammatory activation of macrophages. (A) Two independent strategies, Af1521 and 10H antibody workflows, for ADP-ribosylation proteomics. (B) Antipan ADP-ribose Western blot analysis of IFN-γ-treated THP-1 cells over 24 h. (C) IFN-γ activation replicates: two sets (control or IFN-γ) of macrophage activation were used for the Af1521 workflow, and three sets were used for the 10H antibody workflow. Details about ADPr peptide data acquisition and analysis are highlighted using the second Af1521 replicate of IFN-γ-treated THP-1 cells.

Rank 1 PSMs/peptides were used for further data analysis. Of note, for amino acid site localization probabilities for HCD data, as shown in Figure S3B, when a single replicate was used and the ADPr localization could not be assigned to a given amino acid (e.g., K7 to R9 are candidates as in Figure S3B), Rank 1 peptides were random, and their corresponding probability was scored as high (>95%) rather than the expected 33% given 3 possible amino acid acceptor sites for this particular peptide. On the other hand, when two sets of replicate data were combined, then the probabilities were equally assigned. The feature mapper allowed to perform a retention time alignment and a precursor intensity-based quantification, and the abundance values were normalized by a total peptide amount mode. To search ADPr site motifs, we compared amino acid sequence around ADPr site within a window of 5 amino acids using Weblogo.[45] For an analysis of input samples, we used the settings described in 10H-Dependent Anti-PARylated Immunoprecipitated Peptides below.

10H-Dependent Anti-PARylated Immunoprecipitated Peptides. The MS/MS data were queried against the human UniProt database (downloaded on August 1, 2014) using the SEQUEST-HT search algorithm, via the PD Package (version 2.2), using a 10 ppm tolerance window in the MS1 search space, and a 0.02 Da fragment tolerance window for HCD. Oxidation of M was set as a variable modification, and carbamidomethylation of C was set as a fixed modification. Peptides were filtered on the basis of a 1.0% FDR. Peptides assigned to a given protein group, and not present in any other protein group, were considered as unique. Consequently, each protein group is represented by a single master protein (PD grouping feature). Master proteins with two or more unique peptides were used for precursor ion intensity-based quantification. The normalized abundance values using a total peptide amount mode were exported from the software.

Statistical and Protein−Protein Interaction Network Analyses

All the statistical analyses were done using R (version 3.5.1) in the Rstudio environment (https://www.rstudio.com/). For

graphics, we employed ggplot2[46] and igraph[47] R packages. Pearson's correlation coefficient was calculated for comparison of ADPr peptide and/or protein abundances. Regression analysis was done to explain a correlative relationship between the two Af1521 replicates. We also computed standard error of estimates (SEE) to evaluate regression fits. A 95% confidence interval was used to find outliers (IFN-γ vs control). Protein−protein interaction (PPI) networks were constructed by the STRINGdb[48] R packages (version 1.20.0). We acquired high confidence interactions (STRINGdb confidence interaction scores ≥700: active interaction sources; text mining, experiments, databases, coexpression, neighborhood, gene fusion, and co-occurrence) and hid disconnected proteins from networks. We performed gene ontology (GO) analysis via the PANTHER database[49] to understand biological process of PPI complexes. GO clusters (labeled GO-1 to GO-7) were then input into a word cloud tool, to help consolidate the various GO terms into simpler representatives.

Database Comparison

The gene names of identified 145 ADPr proteins (Af1521 workflow) and 10H enriched 1389 proteins (10H workflow) in our study were compared to three other reported databases.[12,20,50]

Data Availability

The .RAW output files and the exported Proteome Discoverer peptide lists for all Af1521 product ion triggered data, including PRM acquisitions for THP-1 and cell-free reactions, have been deposited to the ProteomeXchange Consortium via PRIDE[51,52] partner repository with the data set identifier PXD011690. Additional data are available from corresponding authors upon request.

■ RESULTS

ADP-Ribosylation Increases during IFN-γ-Induced Proinflammatory Activation of Macrophages

We used two strategies to enrich ADPr protein substrates from the IFN-γ-stimulated human macrophage-like cell line THP-1 (Figure 1A): (1) the Af1521-based workflow that relies on the
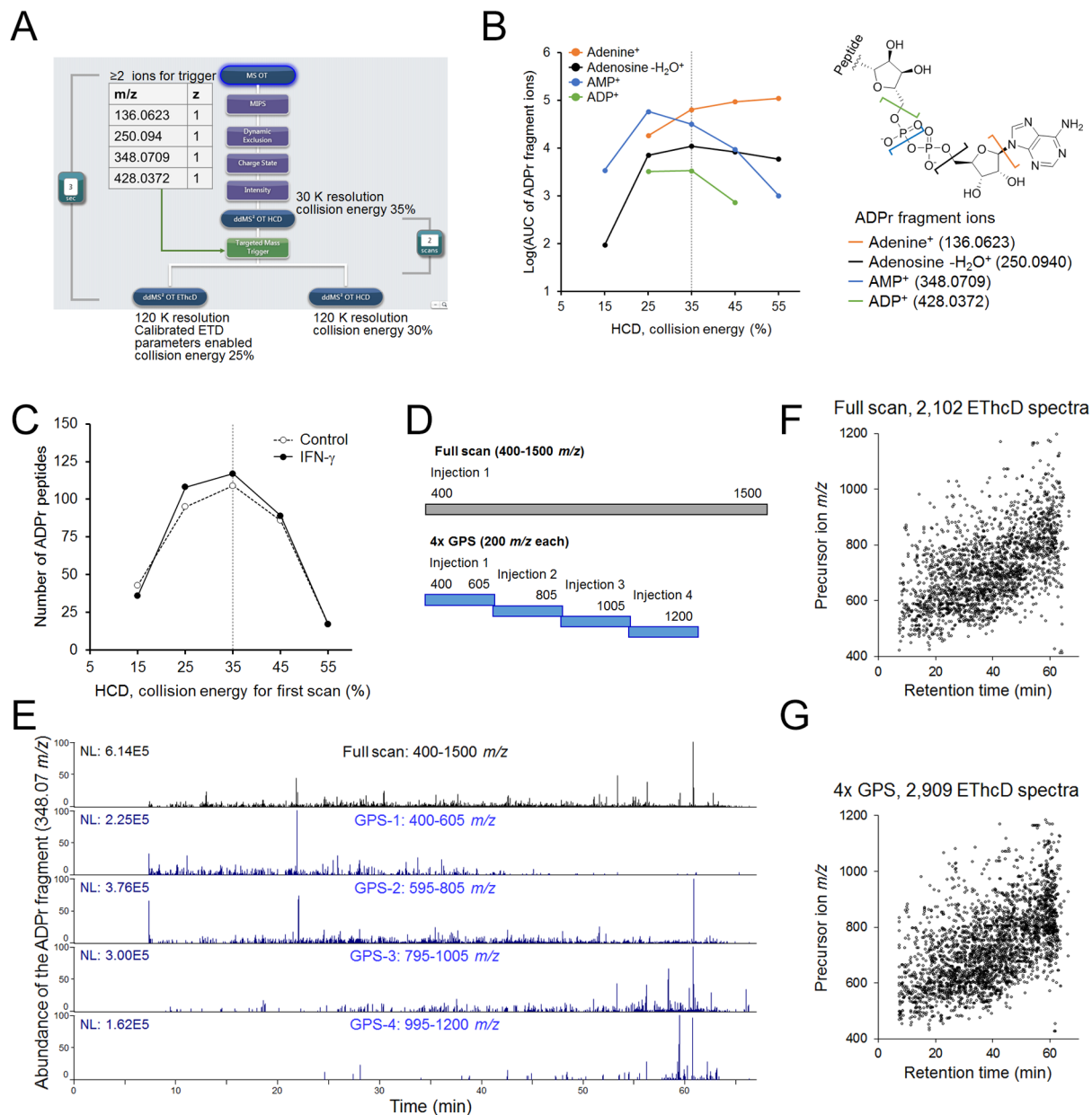
Figure 2. Gas phase segmentation (GPS) improves ADPr peptide detection. (A) A screenshot of the ADP-ribose product ion triggered EThcD and HCD data acquisition method on the Orbitrap Fusion Lumos. (B) Area under the curve (AUC) of the four ADPr fragment ions (136.06, 250.09, 348.07, and 428.04 m/z) dissociated from an ARTD8/PARP14-MARylated STAT1 peptide using HCD. (C) Pilot Af1521 enrichment study to determine the optimal collision energy for ADP-ribose product ion screening and ADPr peptide identification. Only high confidence (HCD and EThcD combined peptides) were used in this plot (more details in Figure 3). (D) A schematic showing the principle of GPS using multiple injections. (E) The extracted ion chromatograms of the ADPr fragment peak (348.07 m/z) in each full scan and GPS injection. (F,G) Precursor ion m/z and retention time of triggered EThcD spectra in full scan and combined GPS scans.

enrichment of MARylated peptides after PARG treatment and (2) the 10H anti-PARylation IP workflow that relies on the enrichment of PARylated proteins. The major difference between the two strategies is that 10H-generated spectra are dominated by backbone peptides, whereas the Af1521-based spectra are rich in MARylated peptides. An antipan ADP-ribose Western blot analysis of IFN-γ-stimulated THP-1 cells over 24 h indicated a peak ADP-ribosylation signal between 6 to 12 h (Figure 1B). We therefore proceeded with the 6-h time point for subsequent proteomics analysis. For the Af1521 strategy, each replicate was a pool of 15 10 cm-dishes of THP-1 cells—two sets of either control or IFN-γ-stimulated cells.

For the 10H strategy, each replicate was a pool of three 10 cm-dishes of THP-1 cells, and we performed three sets (control or IFN-γ) of IP experiments (Figure 1C). The following figures that highlight the various MS acquisition and subsequent interpretation of MS/MS data will be featured using the second replicate of the Af1521 ADPr peptide enrichment (Figure 1C).

Gas Phase Segmentation (GPS) Improves ADPr Peptide Detection

We employed the ADP-ribose product ion triggered method to further enrich ADPr spectra (Figure 2A)[26] within the Af1521-
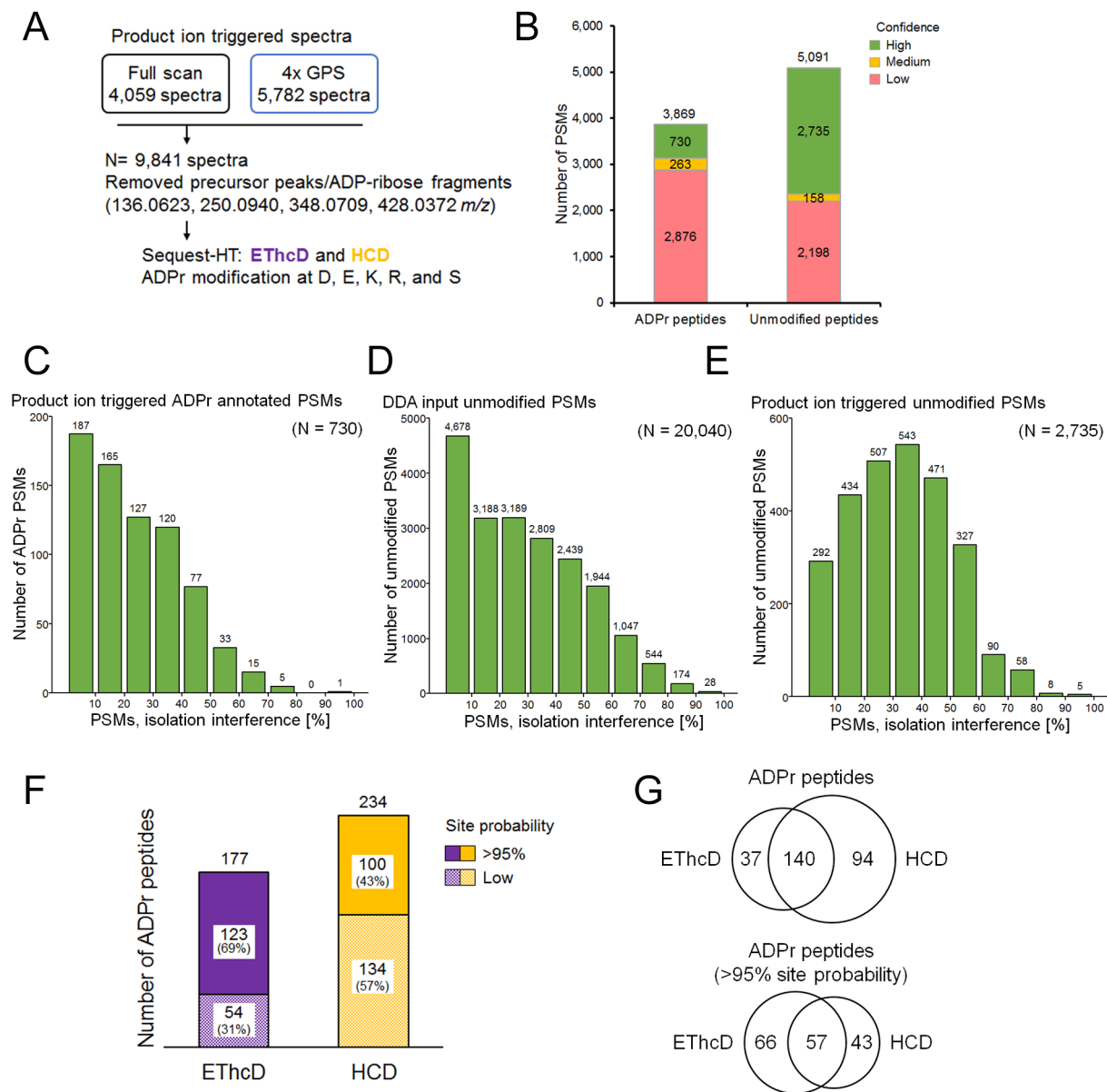
Figure 3. Data processing of product ion triggered MS/MS spectra. (A) A schematic of SEQUEST-HT searches of triggered EThcD and HCD spectra using the second Af1521 replicate of IFN-γ-treated THP-1 cells. (B) Number of peptide-spectrum matches (PSMs) of assigned ADPr and unmodified peptides from the triggered spectra. (C−E) Distribution of isolation interference for product ion triggered or DDA PSMs. (F) Number of ADPr peptides with high confidence detected by either EThcD or HCD. (G) Venn diagrams comparing ADPr peptide identifications between EThcD and HCD for all ADPr peptides, and those with >95% ADPr acceptor site probability.

enriched peptide pool that is known to contain contaminant peptides.[53] The first MS/MS scan relies on HCD with 35% collision energy for optimal fragmentation of the ADPr moiety (Figure 2B) as demonstrated by the AUC of the four ADPr fragment ions (adenine+ 136.0623 *m/z*, adenosine-H_2O^+ 250.0940 *m/z*, AMP+ 348.0709 *m/z*, and ADP+ 428.0372 *m/z*) using a cell-free derived MARylated peptide standard (see Experimental Section);[41] and the second (EThcD, supplemental activation 25% collision energy) and third (HCD, 30% collision energy) scans are triggered when at least two of four ADPr product ions are observed (Figure 2A). This acquisition strategy was optimal for the identification of ADPr peptides, as verified with a pilot Af1521 enrichment study (Figure 2C). We also increased overall signal-to-noise by performing the GPS technique that employs multiple

injections of the sample, but each injection is a 200 *m/z* MS1 survey scan segment increment totaling the mass range of 400 to 1200 *m/z* (Figure 2D). The extracted ion chromatograms of the 348.07 *m/z* peak demonstrate the increased signal per 200 *m/z* mass range when compared to the default full MS survey scan range of 400 to 1500 *m/z* (Figure 2E). As exemplified by the EThcD scans, the total number of triggered events went from 2102 for the full MS survey scan range to 2909 for the combined GPS scan ranges (Figure 2F,G).

Data Processing of Product Ion Triggered MS/MS Spectra

By extracting only the ADP-ribose product ion triggered sequencing events (EThcD and HCD combined), we obtained 4059 spectra from the full MS survey scan and 5782 spectra from the combined GPS scans (Figure 3A). After removing the
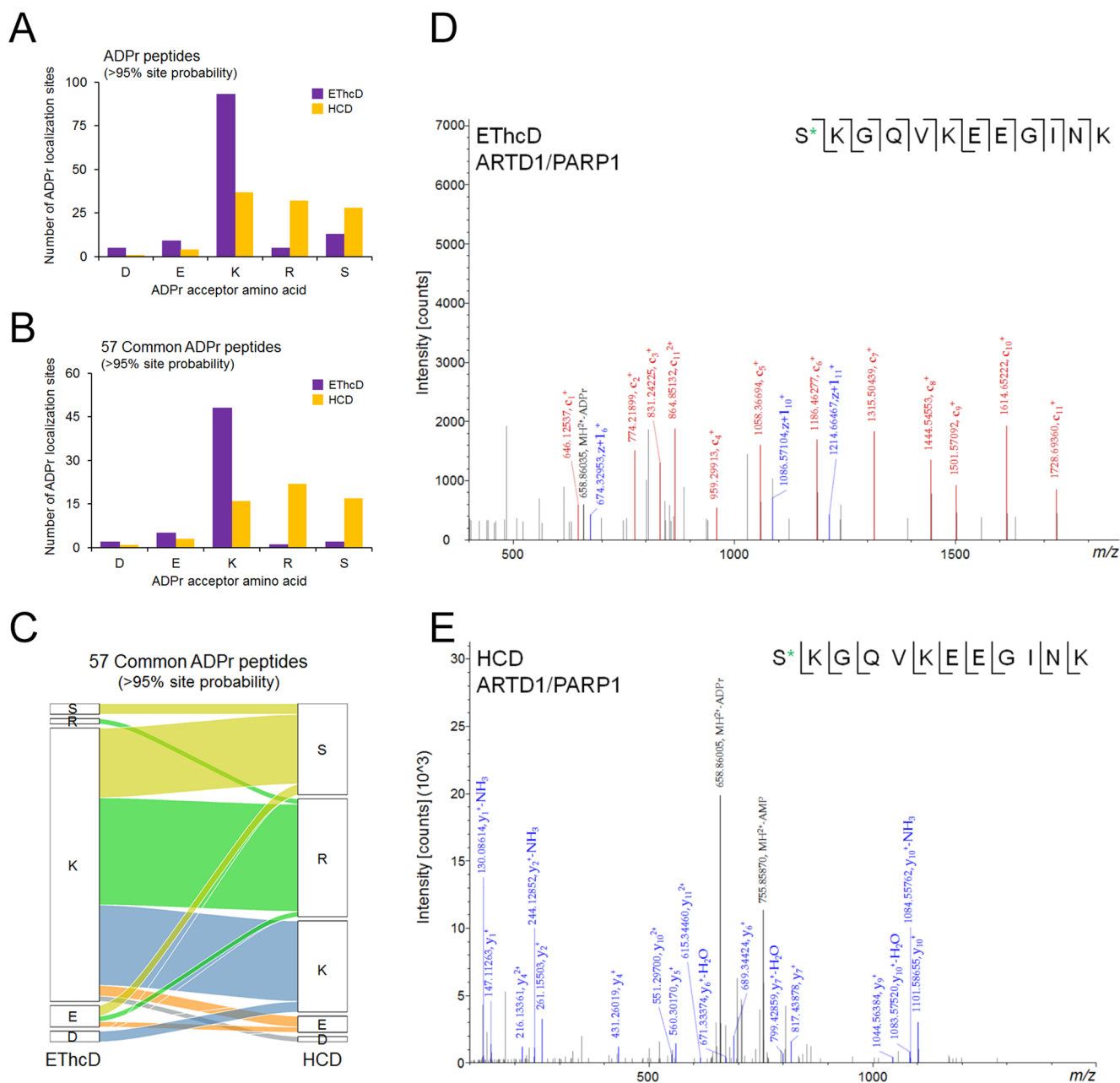
Figure 4. EThcD provides improved ADPr acceptor site localization in THP-1 protein substrates. (A) Distribution of confident ADPr acceptor amino acids (>95% site probability) of all identified ADPr peptides triggered by either EThcD or HCD spectra using the second Af1521 replicate of IFN-γ-treated THP-1 cells. (B) Distribution of confident ADPr acceptor amino acids of the 57 common ADPr peptides (Figure 3G). (C) An alluvial diagram showing conserved or variant assignments between the two activation methods. (D,E) ARTD1/PARP1 ADPr annotated spectra. ADPr-associated peaks (black peaks) were manually annotated. *, ADPr site.

precursor peaks and ADPr fragment ions, EThcD and HCD spectra were separately searched against five amino acid acceptor sites: D, E, K, R, and S (Figure 3A). In total, 8960 peptide-spectrum matches (PSMs) were acquired, of which 3869 were ADPr peptide assignments, whereas 5091 triggered spectra were assigned to unmodified peptides (Figure 3B). Of the ADPr peptides, 730 were ranked as high confidence, 263 were medium, and 2876 were low (Figure 3B). Of the unmodified peptides, 2735 were high confidence, 158 were medium, and 2198 were low (Figure 3B). The high number of unmodified peptide assignments is due to their nonspecific enrichment in the Af1521 workflow (as previously reported[53]),

and subsequent coisolation with ADPr peptides (Figure S2). For instance, the distribution of percent isolation interference for high confidence ADPr PSMs (Figure 3C, median, 21%) resembles that for the input data-dependent acquired (DDA) PSMs (Figure 3D, median, 27%), whereas the distribution is shifted to a higher range (Figure 3E, median, 32%) for the annotated unmodified PSMs in the product ion triggered acquisitions. Although this trigger strategy aims to increase ADPr peptide specificity, there remains sufficient contaminant unmodified peptides to limit this effort.

Breaking down the high confidence ADPr peptides further, 177 were identified using EThcD and 234 using HCD (Figure
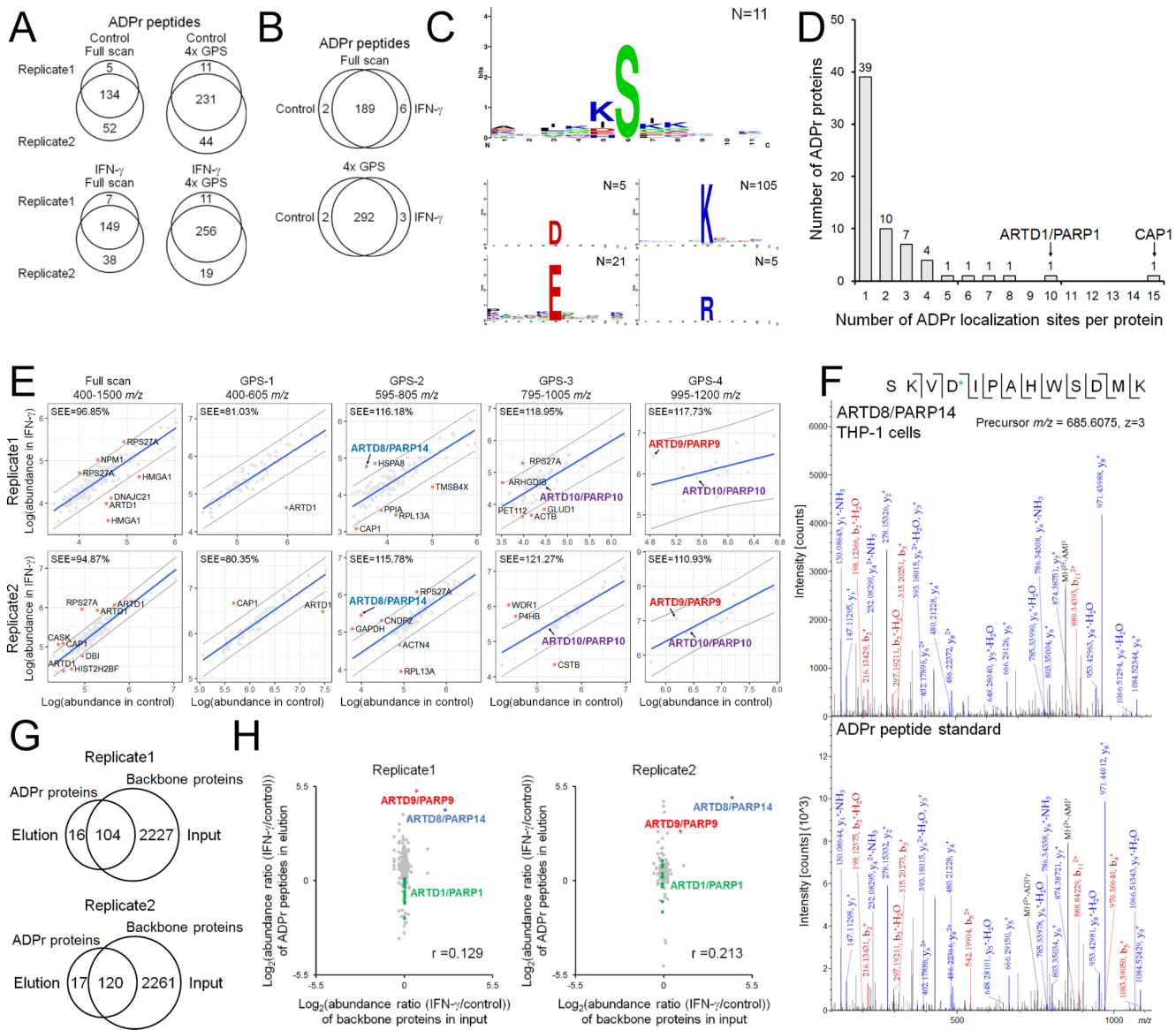
Figure 5. GPS leads to the identification of ADP-ribosylated ARTDs/PARPs other than ARTD1/PARP1. (A) A comparison using Venn diagrams for ADPr peptides found in two replicates for full scan (400−1500 m/z) and combined 4× GPS scans (GPS-1, 400−605; GPS-2, 595−805; GPS-3, 795−1005; GPS-4, 995−1200 m/z). (B) A comparison of ADPr peptides found in control and IFN-γ-treated THP-1 cells for the full scan and combined 4× GPS scans. (C) Sequence motif analysis for ADPr acceptor amino acids (N, number of ADPr peptides used for the analysis). (D) A plot of the number of ADP-ribosylation sites per protein. (E) Comparison of ADPr peptide abundances between control and IFN-γ in each replicate; regression lines, 95% confidence interval, and standard error of estimate (SEE) are provided (red dots are outliers). (F) MS/MS spectra of an ARTD8/PARP14 ADPr peptide using PRM acquisitions. Black peaks were manually annotated. *, ADPr site. (G) A comparison of the number of proteins identified in the Af1521 elution (ADPr proteins) and input samples (backbone proteins) per replicate. (H) A comparison of the relative changes to ADPr peptides versus their backbone proteins in response to IFN-γ (IFN-γ/control).

3F), with 140 overlapping between the two activation methods (Figure 3G). Sixty-nine percent of the EThcD ADPr peptides had >95% probability for the amino acid acceptor site, whereas only 43% of HCD ADPr peptides had high probability for the acceptor site (Figure 3F). Although the HCD method led to more peptide identifications, the EThcD method led to a greater number of confident amino acid acceptor sites (Figure 3G).

EThcD Provides Improved ADPr Acceptor Site Localization in THP-1 Protein Substrates

We next determined whether there was any acceptor site bias between EThcD and HCD activation methods. We focused on

ADPr peptides with >95% ADPr site probability. EThcD spectra gave rise to predominantly K acceptor sites, followed by S, E, D, and R (Figure 4A, Figure S3). On the other hand, HCD spectra resulted in a similar number of acceptor sites at K, R, and S, followed E and D (Figure 4A). Despite limiting the analysis to the 57 commonly detected ADPr peptides that should have the same amino acid assignments, we still observed similar acceptor distribution patterns as in the entire data set (Figure 4B). Using an alluvial diagram to depict conserved versus variant assignments between the two activation methods, we see that EThcD-K sites are equally distributed among the HCD-K, R, and S amino acids; E and D
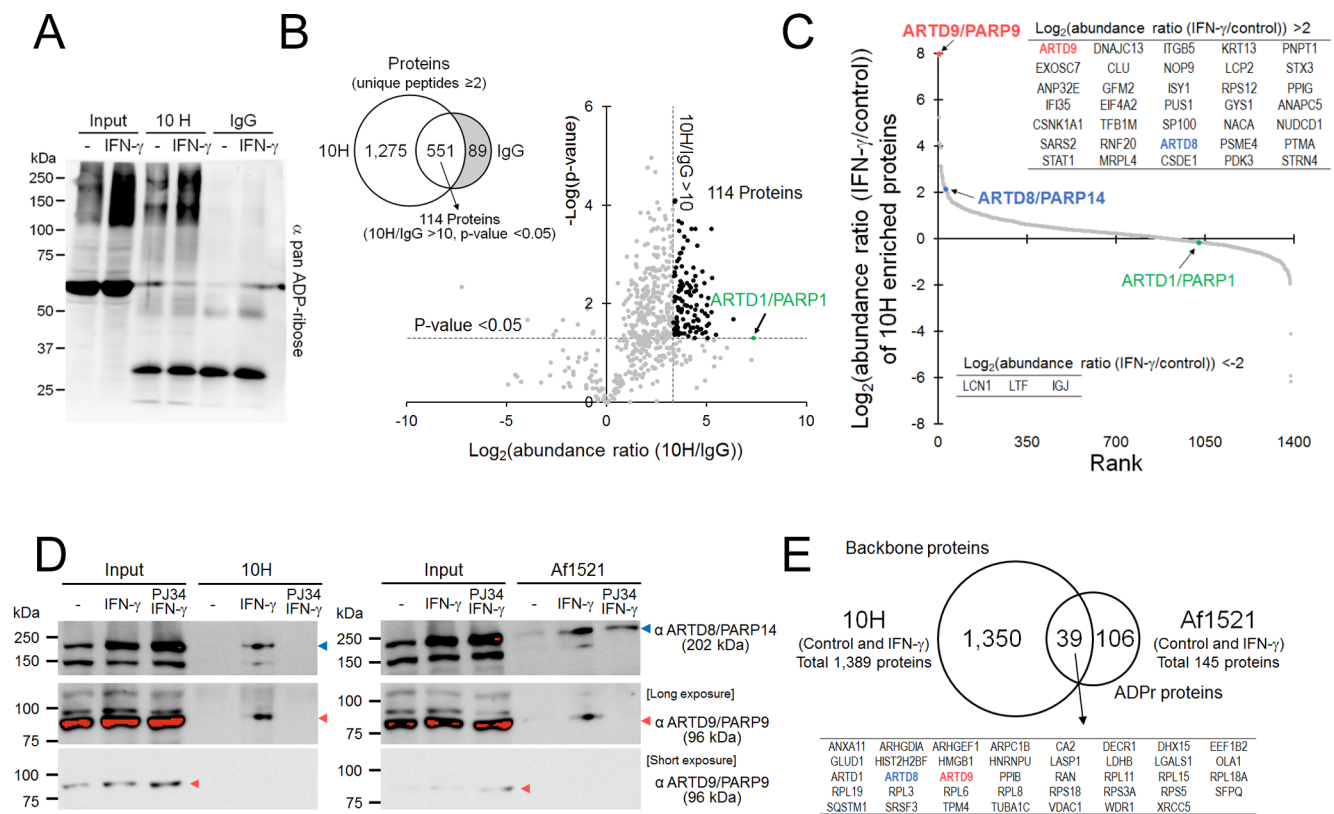
Figure 6. IFN-γ increased ARTD8/PARP14 and ARTD9/PARP9 ADP-ribosylation. (A) A pan ADP-ribose Western blot analysis of control and IFN-γ-treated THP-1 cells after 10H IP or incubation with IgG. (B) A comparison of enriched proteins using a Venn diagram between 10H and IgG. The plot showing the $\log_2$(abundance ratio (10H/IgG)) and $-\log(p$-value) of 551 shared proteins (Venn diagram). 114 proteins passed the threshold of abundance ratio (10H/IgG) > 10-fold and p-value < 0.05. (C) Abundance ratio (IFN-γ/control) of 10H-enriched proteins, ARTD9/PARP9, DNAJC13, and ITGB5, were unique to IFN-γ and filled with maximum. (D) Western blot analysis of Af1521- and 10H antibody-enriched ARTD/PARP enzymes from control, IFN-γ-treated, and PJ34 plus IFN-γ-treated THP-1 cells. (E) Comparing ADP-ribosylome from Af1521 (ADPr proteins) and 10H (backbone proteins) data set and showing the list of 39 common proteins between the two data sets.

also demonstrate discrepancies (Figure 4C). These discrepancies are mostly likely due to the more extensive fragmentation provided by EThcD when compared to HCD.[54] We compared the annotated ADPr spectra acquired from the same precursor ion whose triggered scan numbers are 8565 for EThcD and 8566 for HCD: EThcD provided the C_6^+ and C_7^+ fragments to support ADPr localization to K7 (Figure S3A,B). However, if S and R assignments were made from EThcD data, they were the same in HCD data, as demonstrated by an ARDT1/PARP1 Ser-modified peptide (Figure 4D,E) whose serine was also reported to be ADP-ribosylated in HeLa cell experiments.[53]

GPS Leads to the Identification of ADP-Ribosylated ARTDs/PARPs Other than ARTD1/PARP1

We considered ADPr peptides identified by either EThcD or HCD for quantification of both cell culture replicate experiments. Using the Af1521 strategy, we enriched ADPr peptides from unstimulated (control) and IFN-γ-activated THP-1 cells in duplicate. We first examined the overlap in identified ADPr peptides between replicates and obtained at least 66% overlap, for each full scan and combined GPS data (Figure 5A). We then combined the two replicates and compared the overlap between control and IFN-γ conditions (Figure 5B, Figure S4A). In total, 197 ADPr unique peptides were identified by the full scan, and 297 by using GPS scans (Figure 5B), of which 174 were found in both, for a total of

320 unique peptides (Table S1). In addition, using only the EThcD spectra, we evaluated the amino acid consensus for ADPr acceptor sites (Figure 5C). A "KS" motif emerged from ADPr-S sites, as reported for HeLa cells and mouse embryonic fibroblast cells,[26,29] whereas no clear consensus was evident for the other four amino acids (Figure 5C). These acceptor sites were primarily mapped to unique proteins, for instance, 39 sites came from 39 unique proteins (Figure 5D). At the other end, ARTD1/PARP1 and adenylyl cyclase-associated protein 1 (CAP1) accounted for 10 and 15 unique acceptor sites, respectively (Figure 5D).

We then confirmed that the abundances of commonly identified ADPr peptides correlated between replicates, specifically comparing the quantitative trends between the same sets of full scan and GPS scans (Pearson's r ranged from 0.468 to 0.796, Figure S4B). We then compared ADPr peptide abundances between control and IFN-γ for each replicate separately since the absolute intensities increased in Replicate2. Nonetheless, the similarities in the SEE values indicate that the relative changes between control and IFN-γ are similar (Figure 5E). In each replicate, ARTD1/PARP1 ADPr peptides[55,56] were detected by both full scan and GPS scans; however, the benefit of GPS is best demonstrated by the additional detection of ARTD9/PARP9 and ARTD8/PARP14 ADPr peptides (Figure 5E). To confirm the ARTD9/PARP9 and ARTD8/PARP14 ADPr peptides, we generated a spectral
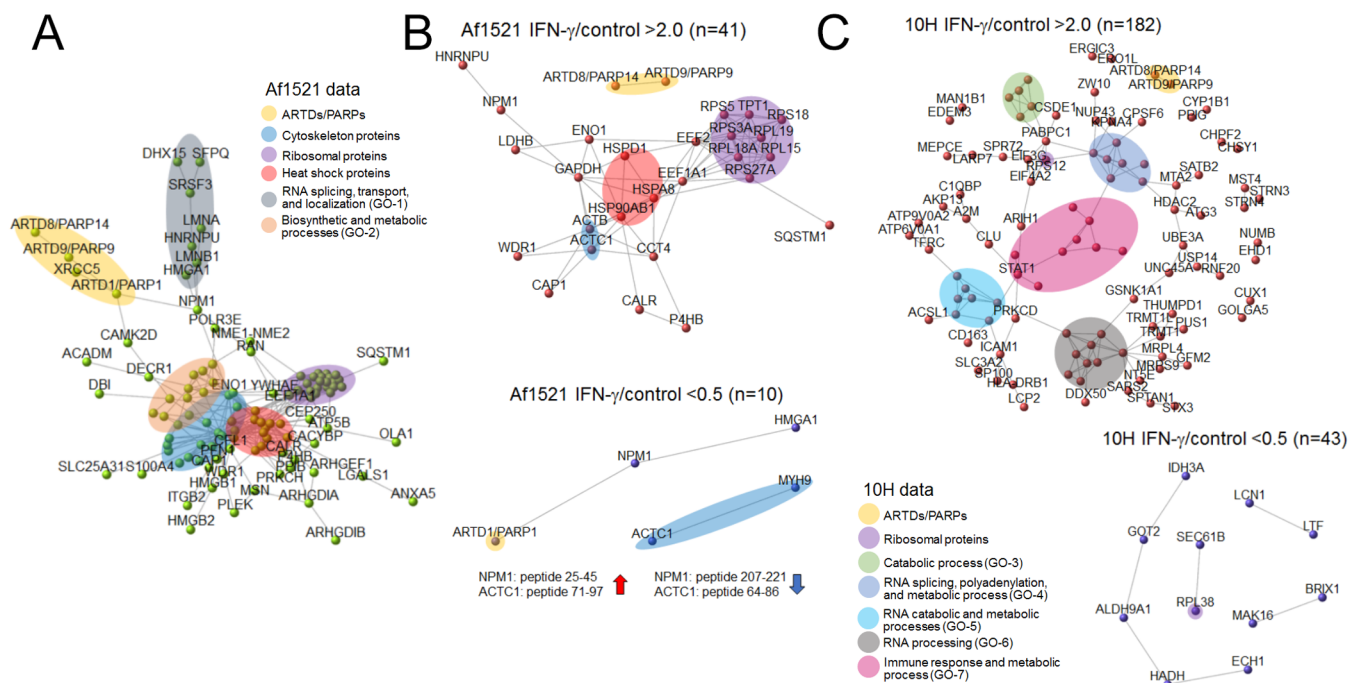
Figure 7. Protein−protein interactions (PPI) in IFN-γ-induced ADP-ribosylome on THP-1 cells. (A) A PPI network mapping all 145 ADPr proteins from Af1521 data and visualizing their interactions (confidence interaction scores ≥700). ADPr proteins with at least one interaction with another ADPr proteins are shown. Selected GO biological processes (GO-1 to GO-7 below) from the extended list in Table S4. (B) PPI networks of 2-fold increased or decreased ADPr proteins in the IFN-γ compared to control. (C) PPI networks from a subset of 2-fold increasing or decreasing enriched proteins using the 10H workflow in response to IFN-γ stimulation.

library using a cell-free ADPr assay (see Experimental Section, Figure S1). We used PRM to increase spectral quality of both standard and THP-1 ADPr peptide samples, and we confirmed the acceptor sites for ARTD8/PARP14 (D1604) and ARTD9/PARP9 (E23) using both HCD and EThcD methods (Figure 5F, Figure S5).

Since we set aside a fraction of the Af1521 input peptides (Figure 1A), we were able to compare the proteomes from each condition and determined that at least 104 ADPr proteins were also detected in the input analysis (Figure 5G, Table S2). We then compared the abundance ratios (IFN-γ/control) of the ADPr peptides with those of their corresponding total proteins from the input samples. There was no correlation (Pearson's r was 0.129 in Replicate1, 0.213 in Replicate2, Figure 5H) between the overall backbone proteome and ADPr peptide abundance, indicating that an increase or decrease in ADPr peptide(s) are less likely due to changes in total protein abundances. However, there are two exceptions in ARTD8/PARP14 and ARTD9/PARP9. Consistent with our previous proteomics kinetics data,[41] IFN-γ-induced ARTD8/PARP14 and ARTD9/PARP9 protein levels increased (e.g., Replicate2, 19.5-fold and 2.07-fold, respectively); however, our current study indicates that their observed ADPr signals were further increased by IFN-γ (e.g., Replicate2, 28.6-fold and 7.36-fold, respectively) (Figure 5H).

IFN-γ Increases ARTD8/PARP14 and ARTD9/PARP9 ADP-Ribosylation

As an independent approach to the Af1521 workflow, we also used the 10H anti-PARylation strategy to immunoprecipitate the PARylated proteome at 6 h of IFN-γ stimulation. After the IP, we evaluated the ADPr signal using an independent detection method (a pan ADP-ribose reagent). Despite

multiple attempts to optimize the IP conditions, the 10H antibody did not recover all ADPr signal as judged by comparison to the input signal, nonetheless, as compared to the IgG control, the 10H antibody was specific to ADPr proteins (Figure 6A). After filtering for proteins with two or more unique peptides, 1275 proteins were unique in 10H, and 551 were overlapped between 10H and IgG data (Figure 6B). Despite the precaution to avoid false positives by using an IgG control, ARTD1/PARP1, the primary PARylating enzyme with auto-ADP-ribosylation activity,[55,56] appeared in the overlap between 10H and IgG (i.e., a false negative). However, ARTD1/PARP1 abundance was greater in the 10H [162-fold (log₂(abundance ratio (IFN-γ/control)) = 7.34) and p-value < 0.05 (−log(p-value) > 1.30)] (Figure 6B). Thus, on the basis of the ARTD1/PARP1 result, we used the cutoff (10H/IgG > 10.0-fold and p-value < 0.05) for the first round of data filtering, resulting in an additional 114 proteins totaling 1389 proteins that were enriched in the 10H condition (Figure 6B). In these data, we observed enrichment of ARTD8/PARP14 (4.48-fold increase) in, and ARTD9/PARP9 unique to, IFN-γ as compared to control, whereas no such change was observed for ARTD1/PARP1 (Figure 6C, Table S3). These trends are consistent with the Af1521 data (Figure 5H).

Nonetheless, on the basis of these mass spectral trends alone, we cannot rule out that the increase in ADPr signal for these two enzymes were due to the increase in overall protein abundance.[50] We therefore performed an additional experiment to support the proteomics findings, which could also at least confirm that both enrichment methods are sensitive to changes in ADP-ribosylation, independent of protein abundance. We treated THP-1 cells with and without IFN-γ for 6 h, and added a third condition that included pretreatment of IFN-γ-stimulated THP-1 cells with a pan-ARTD/PARP

inhibitor (PJ34) (Figure S6A). As demonstrated by the proteomics (Table S2), Western blot analysis confirmed that total ARTD1/PARP1, α-tubulin, GAPDH and HSPD1 levels did not change in response to IFN-γ (Figure S6B). Since GAPDH and HSPD1 ADPr peptides increased in response to IFN-γ (Table S1), the increase in ADP-ribosylation status was not due to changes in their total proteins. Furthermore, the inhibitor did not alter the abundance of these three proteins (Figure S6B). Similarly, the inhibitor did not change the IFN-γ-induced increase in ARTD8/PARP14 and ARTD9/PARP9 (Figure 6D, Figure S6C−F). We then enriched the ADP-ribosylome from these lysates using either Af1521 or the 10H antibody, and performed Western blot analysis against ARTD8/PARP14 and ARTD9/PARP9. In line with the proteomics data (Figure 5E,H, Figure 6C), both enzymes' ADP-ribosyl forms were more enriched in IFN-γ compared to control (Figure 6D). Since a longer exposure time was required to detect the ADP-ribosyl signal in the control lanes, total ARTD9/PARP9 signal was saturated. We thus also provide the shorter exposure time blots that confirms the IFN-γ-dependent increase in protein abundance (Figure 6D). In addition, the PJ34 pretreatment of IFN-γ-stimulated cells, reduced the enrichment of both enzymes' ADP-ribosyl forms (Figure 6D, Figure S6C−F). These data indicate that the increase in ARTD8/PARP14 and ARTD9/PARP9 abundances are not dependent on ADP-ribosylation.

Other candidate ADPr proteins with increased enrichment in IFN-γ include dnaJ homologue subfamily C member 13 (DNAJC13), 40S ribosomal protein S12 (RPS12), anaphase-promoting complex subunit 5 (ANAPC5), and STAT1 (Figure 6C). On the other hand, proteins with decreased enrichment in IFN-γ include lipocalin-1 (LCN1), lactotransferrin (LTF), and immunoglobulin J chain (IGJ) (Figure 6C). Overall, 39 of the 145 Af1521 identified proteins were in common between the Af1521 and 10H studies; however, this is likely due to the incompleteness of the Af1521 peptide identification (Figure 6E).

Protein−Protein Interactions (PPI) in IFN-γ-Induced ADP-Ribosylome on THP-1 Cells

Since this is the first study to characterize the ADP-ribosylome from macrophage-like cells, we performed a PPI network analysis to deduce a potential relationship among ADPr substrate proteins. We selected the 145 ADPr proteins from the Af1521 data, and a subset of increasing and decreasing enriched backbone proteins from the 10H data for network analysis. Regarding the 145 ADPr proteins, we mapped and visualized their interactions (confidence interaction scores ≥700) using the STRING database (Figure 7A). This analysis identified ARTD/PARP-protein interactions: ARTD8/PARP14-ARTD9/PARP9, ARTD9/PARP9-ARTD1/PARP1, ARTD1/PARP1-calcium/calmodulin-dependent protein kinase type II subunit delta (CAMK2D), ARTD1/PARP1-X-ray repair cross-complementing protein 5 (XRCC5), and ARTD1/PARP1-nucleophosmin (NPM1). In addition, proteins pertaining to cytoskeleton, ribosomal, and heat shock complexes were also identified (Figure 7A, unlabeled proteins are listed in Table S4). For other interactions described in the network, their biological processes include RNA splicing, transport, and localization (GO-1), and biosynthetic and metabolic processes (GO-2) (Figure 7A, Table S5 provides all GO terms for each GO-1 to GO-7 below). To clarify potential IFN-γ-induced changes to the ADP-ribosylome, we selected proteins whose

ADPr peptides increased or decreased 2-fold in the Af1521 data set (Figure 7B). Of the 41 proteins with increasing ADP-ribosylation signal, 28 were found to have high confidence interactions, comprising primarily the ribosomal and heat shock proteins (Figure 7B). The decreasing network mapped 5 of 10 proteins, including ARTD1/PARP1 and NPM1 (Figure 7B). Since the PPI network for all 10H identified proteins (1389 proteins) was too cluttered, we simplified the analysis by filtering for those with a 2-fold increase or decrease in IFN-γ. The increasing network mapped approximately 100 of 182 proteins that include the two ARTDs/PARPs (Figure 7C). Other interactions include catabolic process (GO-3); RNA splicing, polyadenylation, and metabolic process (GO-4); RNA catabolic and metabolic processes (GO-5); and RNA processing (GO-6) (Figure 7C). The network also contains immune response and metabolic process terms (GO-7) that are unique to the 10H data set (Figure 7C). The decreasing network generated 11 of 43 proteins (Figure 7C).

We also compared our data to three other ADP-ribosylome studies that each used distinct ADPr enrichment strategies under DNA damaging conditions: Af1521 in HeLa cells,[12] 10H in HeLa and HEK 293 cells,[20] and boronate affinity chromatography in breast cancer cells[50] (Figure S7A). Although these studies were conducted in different cell types and under different conditions, there was overlap in the identified proteins. For instance, the greatest overlap is found between our 145 ADPr proteins and those from the Af1521 in HeLa cell study[12] (21%, Figure S7B), which is reasonable since both studies employed similar enrichment methods. On the other hand, we observed the least overlap with the cancer cell study owing to primarily the specificity of D and E ADPr enrichment by the boronate method[50] (12%, Figure S7B). When comparing all three studies, five proteins are commonly identified as ADP-ribosylated: ARTD1/PARP1, chromosome associated high mobility group protein HMG-I/HMG-Y (HMGA1) and high mobility group protein B2 (HMGB2), heterogeneous nuclear ribonucleoprotein U (HNRNPU), and 60S ribosomal protein L8 (RPL8). Of our 1389 10H enriched proteins, 177 overlap with the 10H ADP-ribosylome in the HeLa and HEK 293 study[20] (13%, Figure S7B), including ARTD1/PARP1, HNRNPU, and RPL8. Only our study, however, reports the identification of ADPr ARTD8/PARP14 and ARTD9/PARP9.

■ DISCUSSION

In recent years, mass spectrometry and proteomics technologies have helped bridge the link between ADP-ribosylation and macrophage biology. Using a tandem mass tagging-based kinetics study, we described the increase of ARTD8/PARP14 and ARTD9/PARP9 protein levels in response to the IFN-γ.[41] However, we did not observe any changes to ARTD1/PARP1 protein levels during macrophage activation. Using in vitro and in vivo experiments, we also demonstrated the anti- and pro-inflammatory properties of ARTD8/PARP14 and ARTD9/PARP9, respectively.[41] In the present study, we further investigated the impact of ADP-ribosylation on macrophage biology by describing, for the first time, not only macrophage protein ADPr acceptor sites, but also those that increase in response to IFN-γ. We relied on two independent approaches to enrich the ADP-ribosylome: enrichment via a classical anti-PARylation antibody, 10H;[17] and enrichment via a very recently developed strategy that capitalizes on the affinity of a macrodomain (Af1521) for ADP-ribosylated substrates.[12] In

the latter, we acquired thousands of ADPr peptide spectra since the workflow directly enriches MARylated peptides; however, as is the case with PTM studies, it requires many cell culture dishes per condition and milligrams of protein input to ensure enrichment. On the other hand, the 10H workflow does not produce any significant ADPr signal (1 or 2 triggered events at best, not shown), and would require a scaled-up workflow that would greatly increase the cost of the antibody, which is not practical for replication experiments.

In order to sequence the backbone and identify ADPr acceptor sites from Af1521-enriched peptides, we relied on multiple activation strategies encompassed in a single mass spectrometric injection. In each scan cycle, a high energy and low resolution HCD scan provides a survey for ADPr product ions, whose presence in turn triggers subsequent EThcD and lower energy HCD acquisitions.[26] Other strategies that include separate injections for HCD, ETD, and/or EThcD would increase the number of analyzed precursors; however, we elected the product ion triggered method since it increases spectral specificity for MARylated peptides. In addition, our acquisition strategy employed separate injections for a series of gas phase segmented mass range survey scans as a means to increase the number of product ion triggered sequencing events. Segmented survey scans are hallmarks for data-independent acquisition (DIA) and sequential window acquisition of all theoretical fragment ion spectra (SWATH) strategies;[57,58] and very recently extended to the BoxCar method that relies on filling the Orbitrap C-trap with sequential segmented scan ranges[59] in lieu of the 1000 to 1500 m/z survey scan range that is typical of standard data-dependent acquisition experiments. Overall, we increased the number of ADPr triggered events and identified ADPr peptides from ARTD9/PARP9, ARTD10/PARP10, and ARTD8/PARP14, that would not have been detected otherwise. Whether these and the other identified ADPr peptides were originally PARylated or MARylated is not yet known since the workflow relies on a PARG hydrolysis step to obtain the mass spectrometric amenable MARylated form of the PTM.

The multiple acquisition and product ion triggered method also permitted us to readily compare and contrast the commonalities and differences between HCD and EThcD on a common precursor. We confirmed previous observations that HCD identifies a greater number of ADPr peptides, whereas EThcD allows reliable ADPr localization.[27] We also observed a previously reported acceptor site motif for EThcD annotated spectra; S-ADPr generally comprises a KS motif,[26] whereas D, E, K, and R-ADPr sites did not yield any apparent consensus motifs (Figure 5). Despite limiting acquisitions to ADPr-containing precursors, less than 10% of MS/MS spectra were confidently assigned as ADPr peptides, and most were annotated as unmodified peptides. These discrepancies are due to multiple confounding factors including, the lack of appropriate annotation methods that account for the various ADPr peptide fragments that dominate MS/MS spectra,[22] and interference from coeluting unmodified peptides. For instance, spectral quality for the ARTD8/PARP14 and ARTD9/PARP9 ADPr peptides was greatly improved with a PRM acquisition that benefited from a smaller isolation window and increased MS/MS resolution across the established retention time of the peptides (Figure 5, Figure S5). The availability of the ADPr peptide standards was important for acceptor site and peptide confirmation. While a follow-up PRM analysis such as this is powerful, it is not practical for the entire ADP-ribosylome.

Thus, the incomplete annotation and prevalence of low confidence identifications of our triggered ADPr spectra limited the identification of additional IFN-γ unique ADPr peptides.

The incomplete annotation of the ADPr spectra is partly responsible for the limited overlap between the Af1521 and 10H data (Figure 6). In addition, the 10H enrichment is not specific to ADPr proteins. For instance, noncovalent interactors via protein−protein or protein-poly-ADPr are expected.[21] Overall, our data are consistent with previous observations that RNA processing and translation machinery proteins are targets of ADP-ribosylation. Our ADP-ribosylome includes a prevalence of RNA processing protein complexes of which several ribosomal ADPr peptides were higher in IFN-γ-elicited THP-1 cells (Figure 7). How these changes impact IFN-γ-induced responses such as cytokine production and release are not apparent in our data. However, we have previously established that ARTD8/PARP14 and ARTD9/PARP9 suppresses and promotes activation of pro-inflammatory signaling in macrophages.[41]

Both Af1521 and 10H ADP-ribosylome data confirmed ADP-ribosylation of ARTD8/PARP14 and ARTD9/PARP9 in THP-1 macrophage-like cells. In addition to an increase in total protein,[41,60] our data indicate that ARTD8/PARP14 and ARTD9/PARP9 ADP-ribosylation statuses also increase in response to IFN-γ (Figures 5 and 6). This increase is independent of the increase in protein abundance as inhibition of global ADP-ribosylation via a pan-ARTD/PARP inhibitor reduced their ADP-ribosyl forms without affecting the IFN-γ-dependent increase in their total proteins. Whether these ADP-ribosylation events were due to ARTD8/PARP14 auto-ADP-ribosylation and trans-ADP-ribosylation of ARTD9/PARP9, cannot be directly determined from these particular experiments. However, our cell-free assays confirm the ability for ARTD8/PARP14 to (auto-)ADP-ribosylate the THP-1 enriched sites (ARTD8/PARP14, D1604; ARTD9/PARP9, E23). It is therefore feasible that, for at least ARTD8/PARP14, its cell-derived ADPr forms are due to its self-modifying activity; that would explain how the observed increase in its ADP-ribosylation status could exceed the increase in its total protein abundance.

CONCLUSIONS

We enriched the ADP-ribosylome from IFN-γ-stimulated THP-1 cells using two independent ADP-ribosylation proteomics strategies: MAR-enriching Af1521-based and anti-PAR 10H antibody immunoprecipitation workflows. This study does not provide information on which ARTD/PARP enzymes promote the increase global ADP-ribosylation in response to IFN-γ; however, it does offer insight into ADP-ribosylated pathways. PPI networks from both Af1521 and 10H enrichment strategies point toward primarily RNA processing complexes, coinciding with previous studies on nuclear ADP-ribosylation. Our study uniquely confirmed a link between IFN-γ and the ADP-ribosylation statuses of ARTD8/PARP14 and ARTD9/PARP9 in macrophages, thereby providing the next steps to understand the roles of these ADP-ribosylated enzyme forms on macrophage activation.

ASSOCIATED CONTENT

S Supporting Information

The Supporting Information is available free of charge on the ACS Publications website at DOI: 10.1021/acs.jproteome.8b00895.

Figures S1−S7 (PDF)
Tables S1−S4 (XLSX)
Table S5 (XLSX)

AUTHOR INFORMATION

Corresponding Authors

*Phone: 617-730-7702. Fax: 617-730-7791. E-mail: sasingh@bwh.harvard.edu.
*Phone: 617-730-7700. Fax: 617-730-7791. E-mail: maikawa@bwh.harvard.edu.

ORCID

Michael O. Hottiger: 0000-0002-7323-2270
Sasha A. Singh: 0000-0003-0929-3164

Author Contributions

[#]S.A.S. and M.A., senior authors, equally contributed to this study. H.H. and S.A.S. performed and oversaw ADP-ribosylation enrichment and mass spectrometry experiments; T.M. performed all cell biology experiments; L.L. contributed to mass spectra data analysis; Y.Y. supported management of this study; M.O.H. provided and consulted on the Af1521 ADP-ribosylation workflow; H.H. and S.A.S. drafted the manuscript; M.A. conceptualized the study, reviewed and edited manuscript, and was responsible for funding.

Notes

The authors declare no competing financial interest.
Additional data have been deposited to the ProteomeXchange Consortium via PRIDE[51,52] partner repository with the data set identifier PXD011690.

ACKNOWLEDGMENTS

REFERENCES

(1) Gupte, R.; Liu, Z.; Kraus, W. L. PARPs and ADP-ribosylation: recent advances linking molecular functions to biological outcomes. *Genes Dev.* **2017**, *31* (2), 101−126.

(2) Hottiger, M. O.; Hassa, P. O.; Luscher, B.; Schuler, H.; Koch-Nolte, F. Toward a unified nomenclature for mammalian ADP-ribosyltransferases. *Trends Biochem. Sci.* **2010**, *35* (4), 208−19.

(3) Hottiger, M. O. Nuclear ADP-Ribosylation and Its Role in Chromatin Plasticity, Cell Differentiation, and Epigenetics. *Annu. Rev. Biochem.* **2015**, *84*, 227−63.

(4) Rosenthal, F.; Hottiger, M. O. Identification of ADP-ribosylated peptides and ADP-ribose acceptor sites. *Front. Biosci., Landmark Ed.* **2014**, *19*, 1041−56.

(5) Leidecker, O.; Bonfiglio, J. J.; Colby, T.; Zhang, Q.; Atanassov, I.; Zaja, R.; Palazzo, L.; Stockum, A.; Ahel, I.; Matic, I. Serine is a new target residue for endogenous ADP-ribosylation on histones. *Nat. Chem. Biol.* **2016**, *12* (12), 998−1000.

(6) Miwa, M.; Sugimura, T. Splitting of the ribose-ribose linkage of poly(adenosine diphosphate-robose) by a calf thymus extract. *J. Biol. Chem.* **1971**, *246* (20), 6362−4.

(7) Oka, S.; Kato, J.; Moss, J. Identification and characterization of a mammalian 39-kDa poly(ADP-ribose) glycohydrolase. *J. Biol. Chem.* **2006**, *281* (2), 705−13.

(8) Feijs, K. L.; Forst, A. H.; Verheugd, P.; Luscher, B. Macrodomain-containing proteins: regulating new intracellular functions of mono(ADP-ribosyl)ation. *Nat. Rev. Mol. Cell Biol.* **2013**, *14* (7), 443−51.

(9) Sharifi, R.; Morra, R.; Appel, C. D.; Tallis, M.; Chioza, B.; Jankevicius, G.; Simpson, M. A.; Matic, I.; Ozkan, E.; Golia, B.; Schellenberg, M. J.; Weston, R.; Williams, J. G.; Rossi, M. N.; Galehdari, H.; Krahn, J.; Wan, A.; Trembath, R. C.; Crosby, A. H.; Ahel, D.; Hay, R.; Ladurner, A. G.; Timinszky, G.; Williams, R. S.; Ahel, I. Deficiency of terminal ADP-ribose protein glycohydrolase TARG1/C6orf130 in neurodegenerative disease. *EMBO J.* **2013**, *32* (9), 1225−37.

(10) Nishizuka, Y.; Ueda, K.; Honjo, T.; Hayaishi, O. Enzymic adenosine diphosphate ribosylation of histone and poly adenosine diphosphate ribose synthesis in rat liver nuclei. *J. Biol. Chem.* **1968**, *243* (13), 3765−7.

(11) Robinson, E. A.; Maxwell, E. S. Chemical properties of elongation factor 2. Amino acid composition, NH 2 -terminal residue, and sulfhydryl reactivity. *J. Biol. Chem.* **1972**, *247* (21), 7023−8.

(12) Martello, R.; Leutert, M.; Jungmichel, S.; Bilan, V.; Larsen, S. C.; Young, C.; Hottiger, M. O.; Nielsen, M. L. Proteome-wide identification of the endogenous ADP-ribosylome of mammalian cells and tissue. *Nat. Commun.* **2016**, *7*, 12917.

(13) Zhang, Y.; Wang, J.; Ding, M.; Yu, Y. Site-specific characterization of the Asp- and Glu-ADP-ribosylated proteome. *Nat. Methods* **2013**, *10* (10), 981−4.

(14) Daniels, C. M.; Ong, S. E.; Leung, A. K. Phosphoproteomic approach to characterize protein mono- and poly(ADP-ribosyl)ation sites from cells. *J. Proteome Res.* **2014**, *13* (8), 3510−22.

(15) Zhen, Y.; Yu, Y. Proteomic Analysis of the Downstream Signaling Network of PARP1. *Biochemistry* **2018**, *57* (4), 429−440.

(16) Rosenthal, F.; Feijs, K. L.; Frugier, E.; Bonalli, M.; Forst, A. H.; Imhof, R.; Winkler, H. C.; Fischer, D.; Caflisch, A.; Hassa, P. O.; Luscher, B.; Hottiger, M. O. Macrodomain-containing proteins are new mono-ADP-ribosylhydrolases. *Nat. Struct. Mol. Biol.* **2013**, *20* (4), 502−7.

(17) Kawamitsu, H.; Hoshino, H.; Okada, H.; Miwa, M.; Momoi, H.; Sugimura, T. Monoclonal antibodies to poly(adenosine diphosphate ribose) recognize different structures. *Biochemistry* **1984**, *23* (16), 3771−7.

(18) Gagne, J. P.; Isabelle, M.; Lo, K. S.; Bourassa, S.; Hendzel, M. J.; Dawson, V. L.; Dawson, T. M.; Poirier, G. G. Proteome-wide identification of poly(ADP-ribose) binding proteins and poly(ADP-ribose)-associated protein complexes. *Nucleic Acids Res.* **2008**, *36* (22), 6959−76.

(19) Isabelle, M.; Gagne, J. P.; Gallouzi, I. E.; Poirier, G. G. Quantitative proteomics and dynamic imaging reveal that G3BP-mediated stress granule assembly is poly(ADP-ribose)-dependent following exposure to MNNG-induced DNA alkylation. *J. Cell Sci.* **2012**, *125* (19), 4555−66.

(20) Gagne, J. P.; Pic, E.; Isabelle, M.; Krietsch, J.; Ethier, C.; Paquet, E.; Kelly, I.; Boutin, M.; Moon, K. M.; Foster, L. J.; Poirier, G. G. Quantitative proteomics profiling of the poly(ADP-ribose)-related response to genotoxic stress. *Nucleic Acids Res.* **2012**, *40* (16), 7788−805.

(21) Daniels, C. M.; Ong, S. E.; Leung, A. K. The Promise of Proteomics for the Study of ADP-Ribosylation. *Mol. Cell* **2015**, *58* (6), 911−24.

(22) Hengel, S. M.; Shaffer, S. A.; Nunn, B. L.; Goodlett, D. R. Tandem mass spectrometry investigation of ADP-ribosylated kemptide. *J. Am. Soc. Mass Spectrom.* **2009**, *20* (3), 477−83.

(23) Rosenthal, F.; Messner, S.; Roschitzki, B.; Gehrig, P.; Nanni, P.; Hottiger, M. O. Identification of distinct amino acids as ADP-ribose

acceptor sites by mass spectrometry. *Methods Mol. Biol.* **2011**, *780*, 57–66.

(24) Zee, B. M.; Garcia, B. A. Electron transfer dissociation facilitates sequencing of adenosine diphosphate-ribosylated peptides. *Anal. Chem.* **2010**, *82* (1), 28–31.

(25) Rosenthal, F.; Nanni, P.; Barkow-Oesterreicher, S.; Hottiger, M. O. Optimization of LTQ-Orbitrap Mass Spectrometer Parameters for the Identification of ADP-Ribosylation Sites. *J. Proteome Res.* **2015**, *14* (9), 4072–9.

(26) Bilan, V.; Leutert, M.; Nanni, P.; Panse, C.; Hottiger, M. O. Combining Higher-Energy Collision Dissociation and Electron-Transfer/Higher-Energy Collision Dissociation Fragmentation in a Product-Dependent Manner Confidently Assigns Proteomewide ADP-Ribose Acceptor Sites. *Anal. Chem.* **2017**, *89* (3), 1523–1530.

(27) Leslie Pedrioli, D. M.; Leutert, M.; Bilan, V.; Nowak, K.; Gunasekera, K.; Ferrari, E.; Imhof, R.; Malmstrom, L.; Hottiger, M. O. Comprehensive ADP-ribosylome analysis identifies tyrosine as an ADP-ribose acceptor site. *EMBO Rep.* **2018**, *19* (8), e45310.

(28) Bilan, V.; Selevsek, N.; Kistemaker, H. A. V.; Abplanalp, J.; Feurer, R.; Filippov, D. V.; Hottiger, M. O. New Quantitative Mass Spectrometry Approaches Reveal Different ADP-ribosylation Phases Dependent On the Levels of Oxidative Stress. *Mol. Cell. Proteomics* **2017**, *16* (5), 949–958.

(29) Abplanalp, J.; Leutert, M.; Frugier, E.; Nowak, K.; Feurer, R.; Kato, J.; Kistemaker, H. V. A.; Filippov, D. V.; Moss, J.; Caflisch, A.; Hottiger, M. O. Proteomic analyses identify ARH3 as a serine mono-ADP-ribosylhydrolase. *Nat. Commun.* **2017**, *8* (1), 2055.

(30) Schreiber, V.; Dantzer, F.; Ame, J. C.; de Murcia, G. Poly(ADP-ribose): novel functions for an old molecule. *Nat. Rev. Mol. Cell Biol.* **2006**, *7* (7), 517–28.

(31) Curtin, N. J.; Szabo, C. Therapeutic applications of PARP inhibitors: anticancer therapy and beyond. *Mol. Aspects Med.* **2013**, *34* (6), 1217–56.

(32) Berton, G.; Sorio, C.; Laudanna, C.; Menegazzi, M.; Carcereri De Prati, A.; Suzuki, H. Activation of human monocyte-derived macrophages by interferon gamma is accompanied by increase of poly(ADP-ribose) polymerase activity. *Biochim. Biophys. Acta, Mol. Cell Res.* **1991**, *1091* (1), 101–9.

(33) Schraufstatter, I. U.; Hyslop, P. A.; Hinshaw, D. B.; Spragg, R. G.; Sklar, L. A.; Cochrane, C. G. Hydrogen peroxide-induced injury of cells and its prevention by inhibitors of poly(ADP-ribose) polymerase. *Proc. Natl. Acad. Sci. U. S. A.* **1986**, *83* (13), 4908–12.

(34) Singh, N.; Poirier, G.; Cerutti, P. Tumor promoter phorbol-12-myristate-13-acetate induces poly ADP-ribosylation in human monocytes. *Biochem. Biophys. Res. Commun.* **1985**, *126* (3), 1208–14.

(35) Kanai, Y.; Miwa, M.; Matsushima, T.; Sugimura, T. Studies on anti-poly(adenosine diphosphate ribose) antibody. *Biochem. Biophys. Res. Commun.* **1974**, *59* (1), 300–6.

(36) Jijon, H. B.; Churchill, T.; Malfair, D.; Wessler, A.; Jewell, L. D.; Parsons, H. G.; Madsen, K. L. Inhibition of poly(ADP-ribose) polymerase attenuates inflammation in a model of chronic colitis. *Am. J. Physiol Gastrointest Liver Physiol* **2000**, *279* (3), G641–51.

(37) Pellat-Deceunynck, C.; Wietzerbin, J.; Drapier, J. C. Nicotinamide inhibits nitric oxide synthase mRNA induction in activated macrophages. *Biochem. J.* **1994**, *297* (1), 53–8.

(38) Eckei, L.; Krieg, S.; Butepage, M.; Lehmann, A.; Gross, A.; Lippok, B.; Grimm, A. R.; Kummerer, B. M.; Rossetti, G.; Luscher, B.; Verheugd, P. The conserved macrodomains of the non-structural proteins of Chikungunya virus and other pathogenic positive strand RNA viruses function as mono-ADP-ribosylhydrolases. *Sci. Rep.* **2017**, *7*, 41746.

(39) Welsby, I.; Hutin, D.; Gueydan, C.; Kruys, V.; Rongvaux, A.; Leo, O. PARP12, an interferon-stimulated gene involved in the control of protein translation and inflammation. *J. Biol. Chem.* **2014**, *289* (38), 26642–57.

(40) Cho, S. H.; Goenka, S.; Henttinen, T.; Gudapati, P.; Reinikainen, A.; Eischen, C. M.; Lahesmaa, R.; Boothby, M. PARP-14, a member of the B aggressive lymphoma family, transduces survival signals in primary B cells. *Blood* **2009**, *113* (11), 2416–25.

(41) Iwata, H.; Goettsch, C.; Sharma, A.; Ricchiuto, P.; Goh, W. W.; Halu, A.; Yamada, I.; Yoshida, H.; Hara, T.; Wei, M.; Inoue, N.; Fukuda, D.; Mojcher, A.; Mattson, P. C.; Barabasi, A. L.; Boothby, M.; Aikawa, E.; Singh, S. A.; Aikawa, M. PARP9 and PARP14 cross-regulate macrophage activation via STAT1 ADP-ribosylation. *Nat. Commun.* **2016**, *7*, 12849.

(42) Bai, P. Biology of Poly(ADP-Ribose) Polymerases: The Factotums of Cell Maintenance. *Mol. Cell* **2015**, *58* (6), 947–58.

(43) Larsen, S. C.; Leutert, M.; Bilan, V.; Martello, R.; Jungmichel, S.; Young, C.; Hottiger, M. O.; Nielsen, M. L. Proteome-Wide Identification of In Vivo ADP-Ribose Acceptor Sites by Liquid Chromatography-Tandem Mass Spectrometry. *Methods Mol. Biol.* **2017**, *1608*, 149–162.

(44) Kennedy, J.; Yi, E. C. Use of gas-phase fractionation to increase protein identifications: application to the peroxisome. *Methods Mol. Biol.* **2008**, *432*, 217–28.

(45) Crooks, G. E.; Hon, G.; Chandonia, J. M.; Brenner, S. E. WebLogo: a sequence logo generator. *Genome Res.* **2004**, *14* (6), 1188–90.

(46) Hadley, W. Ggplot2; Springer Science+Business Media, LLC: New York, NY, 2016.

(47) Csardi, G.; Nepusz, T. The igraph software package for complex network research. *InterJournal* **2006**, 1695.

(48) Franceschini, A.; Szklarczyk, D.; Frankild, S.; Kuhn, M.; Simonovic, M.; Roth, A.; Lin, J.; Minguez, P.; Bork, P.; von Mering, C.; Jensen, L. J. STRING v9.1: protein-protein interaction networks, with increased coverage and integration. *Nucleic Acids Res.* **2012**, *41*, D808–15.

(49) Thomas, P. D.; Campbell, M. J.; Kejariwal, A.; Mi, H.; Karlak, B.; Daverman, R.; Diemer, K.; Muruganujan, A.; Narechania, A. PANTHER: a library of protein families and subfamilies indexed by function. *Genome Res.* **2003**, *13* (9), 2129–41.

(50) Zhen, Y.; Zhang, Y.; Yu, Y. A Cell-Line-Specific Atlas of PARP-Mediated Protein Asp/Glu-ADP-Ribosylation in Breast Cancer. *Cell Rep.* **2017**, *21* (8), 2326–2337.

(51) Vizcaino, J. A.; Csordas, A.; del-Toro, N.; Dianes, J. A.; Griss, J.; Lavidas, I.; Mayer, G.; Perez-Riverol, Y.; Reisinger, F.; Ternent, T.; Xu, Q. W.; Wang, R.; Hermjakob, H. 2016 update of the PRIDE database and its related tools. *Nucleic Acids Res.* **2016**, *44* (D1), D447–56.

(52) Deutsch, E. W.; Csordas, A.; Sun, Z.; Jarnuczak, A.; Perez-Riverol, Y.; Ternent, T.; Campbell, D. S.; Bernal-Llinares, M.; Okuda, S.; Kawano, S.; Moritz, R. L.; Carver, J. J.; Wang, M.; Ishihama, Y.; Bandeira, N.; Hermjakob, H.; Vizcaino, J. A. The ProteomeXchange consortium in 2017: supporting the cultural change in proteomics public data deposition. *Nucleic Acids Res.* **2017**, *45* (D1), D1100–D1106.

(53) Larsen, S. C.; Hendriks, I. A.; Lyon, D.; Jensen, L. J.; Nielsen, M. L. Systems-wide Analysis of Serine ADP-Ribosylation Reveals Widespread Occurrence and Site-Specific Overlap with Phosphorylation. *Cell Rep.* **2018**, *24* (9), 2493–2505.

(54) Frese, C. K.; Altelaar, A. F.; van den Toorn, H.; Nolting, D.; Griep-Raming, J.; Heck, A. J.; Mohammed, S. Toward full peptide sequence coverage by dual fragmentation combining electron-transfer and higher-energy collision dissociation tandem mass spectrometry. *Anal. Chem.* **2012**, *84* (22), 9668–73.

(55) Ogata, N.; Ueda, K.; Kawaichi, M.; Hayaishi, O. Poly(ADP-ribose) synthetase, a main acceptor of poly(ADP-ribose) in isolated nuclei. *J. Biol. Chem.* **1981**, *256* (9), 4135–7.

(56) Langelier, M. F.; Planck, J. L.; Roy, S.; Pascal, J. M. Structural basis for DNA damage-dependent poly(ADP-ribosyl)ation by human PARP-1. *Science* **2012**, *336* (6082), 728–32.

(57) Gillet, L. C.; Navarro, P.; Tate, S.; Rost, H.; Selevsek, N.; Reiter, L.; Bonner, R.; Aebersold, R. Targeted data extraction of the MS/MS spectra generated by data-independent acquisition: a new concept for consistent and accurate proteome analysis. *Mol. Cell. Proteomics* **2012**, *11* (6), O111 016717.

(58) Venable, J. D.; Dong, M. Q.; Wohlschlegel, J.; Dillin, A.; Yates, J. R. Automated approach for quantitative analysis of complex peptide

mixtures from tandem mass spectra. *Nat. Methods* **2004**, *1* (1), 39–45.

(59) Meier, F.; Geyer, P. E.; Virreira Winter, S.; Cox, J.; Mann, M. BoxCar acquisition method enables single-shot proteomics at a depth of 10,000 proteins in 100 minutes. *Nat. Methods* **2018**, *15*, 440.

(60) Caprara, G.; Prosperini, E.; Piccolo, V.; Sigismondo, G.; Melacarne, A.; Cuomo, A.; Boothby, M.; Rescigno, M.; Bonaldi, T.; Natoli, G. PARP14 Controls the Nuclear Accumulation of a Subset of Type I IFN-Inducible Proteins. *J. Immunol.* **2018**, *200* (7), 2439–2454.